Formation of Structure of an Annealed High-Speed Steel upon Laser Surface Melting

Preprint *in* The Physics of Metals and Metallography · April 2019

DOI: 10.1134/S0031918X19040033

5 authors, including:

Ľubomír Čaplovič
Slovak University of Technology in Bratislava
96 PUBLICATIONS **871** CITATIONS

SEE PROFILE

Victor Myshkovets
Francisk Skorina Gomel State University
10 PUBLICATIONS **9** CITATIONS

SEE PROFILE

ISSN 0031-918X, Physics of Metals and Metallography, 2019, Vol. 120, No. 4, pp. 371–377. © Pleiades Publishing, Ltd., 2019.
Russian Text © A.S. Chaus, A.V. Maksimenko, N.N. Fedosenko, Ľ. Čaplovič, V.N. Myshkovets, 2019, published in Fizika Metallov i Metallovedenie, 2019, Vol. 120, No. 4, pp. 400–407.

STRUCTURE, PHASE TRANSFORMATIONS, AND DIFFUSION

Formation of Structure of an Annealed High-Speed Steel upon Laser Surface Melting

A. S. Chaus[a], *, A. V. Maksimenko[b], N. N. Fedosenko[b], Ľ. Čaplovič[a], and V. N. Myshkovets[b]

[a] *Faculty of Materials Science and Technology, Slovak University of Technology, Trnava, 917 24 Slovakia*

[b] *Francisk Skorina Gomel State University, Gomel, 246019 Republic of Belarus*

**e-mail: alexander.chaus@stuba.sk*

Received April 28, 2018; revised November 13, 2018; accepted November 21, 2018

Abstract—The effect of the time and energy parameters of pulsed laser treatment on the structure formation and hardness of high-speed steel after annealing upon surface melting has been studied. The results of the metallographic analysis and energy-dispersive X-ray microanalysis of the steel, as well as of the microhardness measurements, have been discussed. It has been shown that the laser-induced remelting of the annealed high-speed steel causes a significant refinement of both the solid solution and of the carbide constituent. The structure of the laser-affected zone and the morphology of dendrites depend on the laser-irradiation regimes.

Keywords: high-speed steel, laser remelting, microstructure, microhardness

DOI: 10.1134/S0031918X19040033

INTRODUCTION

Despite ever-increasing competition from hard alloys, cutting ceramics, and superhard tool materials, high-speed steels (HSSs) are widely used for the production of a certain type of metal-cutting tool [1]. This is due to their higher toughness and strength as compared to the above-mentioned tool materials [2, 3]. Different methods for strengthening the surface layer of HSSs have been developed and introduced. The most widespread methods are chemical vapor deposition (CVD) [4–7], physical vapor deposition (PVD) [8–11], chemical heat treatment [12–17], and laser treatment (LT) [18–30] of the surface, including selective laser melting, which makes it possible to obtain products of complicated geometric shape by sequential and selective layer-by-layer remelting of the initial material [31, 32], including high-alloy steels for tools of complicated shape [31].

The effects of the energy and the velocity of surface scanning were studied in the published works, usually upon continuous LT [22, 23, 25–27] and (significantly less frequently) upon pulsed LT [24, 28] of the heat-treated HSSs. However, these studies contain no data on whether there are differences in the formation of the microstructure upon LT when the HSS is in the annealed or in a heat-treated state, and whether there is an effect of the time distribution of the energy flux in the laser-irradiation pulses.

In this regard, in [33] we studied the effect of specific regimes of pulsed LT on the structure formation and hardness of the HSS upon surface melting after full heat treatment. The present paper aims to study the features of structure formation and changes in hardness upon laser surface melting of the annealed HSS with a similar chemical composition.

EXPERIMENTAL

The annealed HSS of grade P6M5 (Russian Standard GOST 19265–73) was subjected to laser treatment. The samples 10 mm in height obtained from the annealed rolled rod with a diameter of 30 mm and a hardness of 272 HV (O-series samples) were used. The samples were subjected to isothermal annealing at 850°C for at least 2 h followed by cooling to 720°C and holding for 4 h. The cooling to 500°C was performed in a furnace and then in air. The remelting of the surface of the samples was carried out using a laser technological setup with parameters described in [33].

We used the variant of the time distribution of the energy flux in the laser-irradiation pulses to create triangular shapes of the pulses: with a steep leading front and a slowly decreasing trailing front (Fig. 1). The time and energy parameters of the laser irradiation are given in Table 1.

The microstructure was studied using a JEOL JSM-7600F scanning electron microscope equipped with an Oxford Instruments attachment for energy-dispersive X-ray spectroscopy. The samples for metallographic studies were cut and prepared according to the standard method using Buehler equipment and consumable products. For scanning electron microscopy, unetched samples were used.

Table 1. Time and energy parameters of the laser irradiation

Sample	Frequency, Hz	Duration × 10^{-3}, s	Energy, J
O1	3	3	10
O2	3	9	14
O3	3	18	19

The volume fraction of residual austenite in the structure of the steel was determined using an optical microscope and a NIS-Elements software at a standard 800-fold magnification. The samples were etched in a 4% nital solution. Five measurements were performed for each sample.

The microhardness was measured using a Buehler IndentaMet 1105 tester under a load of 100 g (*HV* 0.1) for 10 s. Ten measurements were performed for each sample. The microhardness was determined as an arithmetic average.

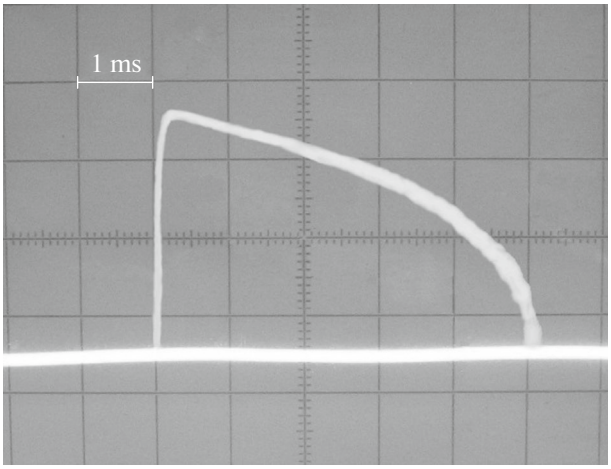

Fig. 1. Oscillogram of the time distribution of the energy flux in the laser-irradiation pulses in the case of a triangular shape of the pulses with a steep leading front and a slowly decreasing trailing front.

RESULTS AND DISCUSSION

The microstructure of the rolled P6M5 HSS in the as-annealed state is represented by a eutectoid mixture of ferrite and carbides, as well as by particles of coarser eutectic carbides grained upon hot plastic deformation (Fig. 2a). In Fig. 2b, two types of carbide particles can be seen: dark and bright. The chemical composition of dark particles corresponds to MC carbide; that of bright particles, to M_6C carbide [34].

Figure 3 shows the overall view of the structure of the laser-affected zone (LAZ) of samples of the O series. As can be seen from Table 2, the depth and width of the LAZ are in the range of 83–280 and 1196–1497 μm, respectively. The metallographic analysis of samples (Fig. 3) showed that the microstructure of the remelting zone (RMZ) in all the cases had apparent signs of directional crystallization and was formed mainly by columnar dendrites with poor etchability, which confirms the presence of large temperature gradients in the structure formation zone. It should be noted that a similar microstructure of the RMZ was detected in the heat-treated HSS after laser surface melting using minimum duration and energy of the pulse with a similar variant of the time distribution of the energy flux [33]. A typical feature of such a microstructure is the presence of dendrites with long primary axes. Their secondary axes in the transverse section have the form of slightly elongated hexagonal cells, which was confirmed in the case of the LT of the annealed steel on the example of O1 (Figs. 4a, 4b) and O3 (Figs. 4c, 4d) samples. It should be noted that the microstructure of the HSS in the as-annealed state after LT is characterized by a higher degree of dispersion in comparison with samples of the heat-treated HSS [33]. In many cases, the cell size in the HSS in the as-annealed state is about 500 nm; the size of car-

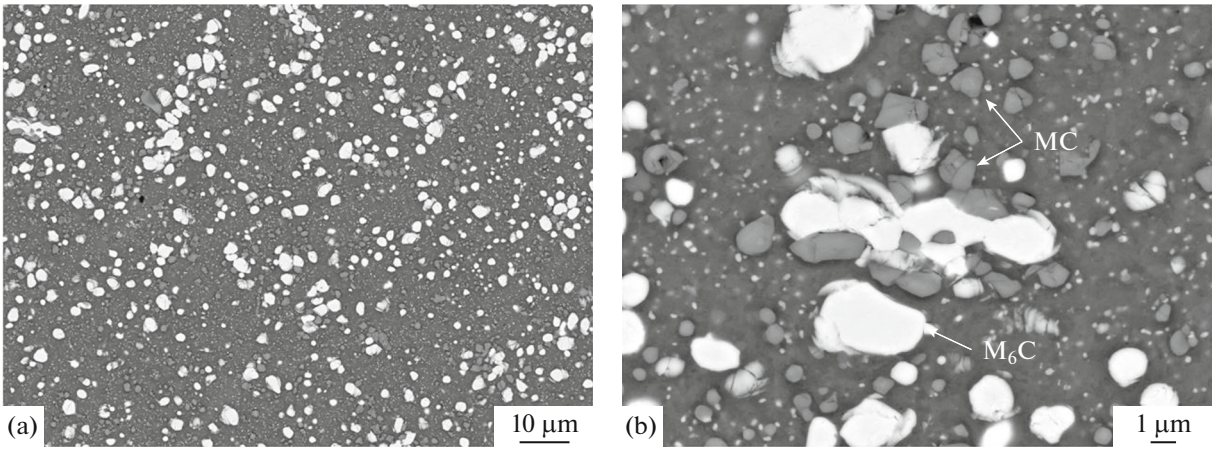

Fig. 2. Image of the microstructure of the annealed high-speed steel of grade P6M5 at (a) lower and (b) higher magnification.

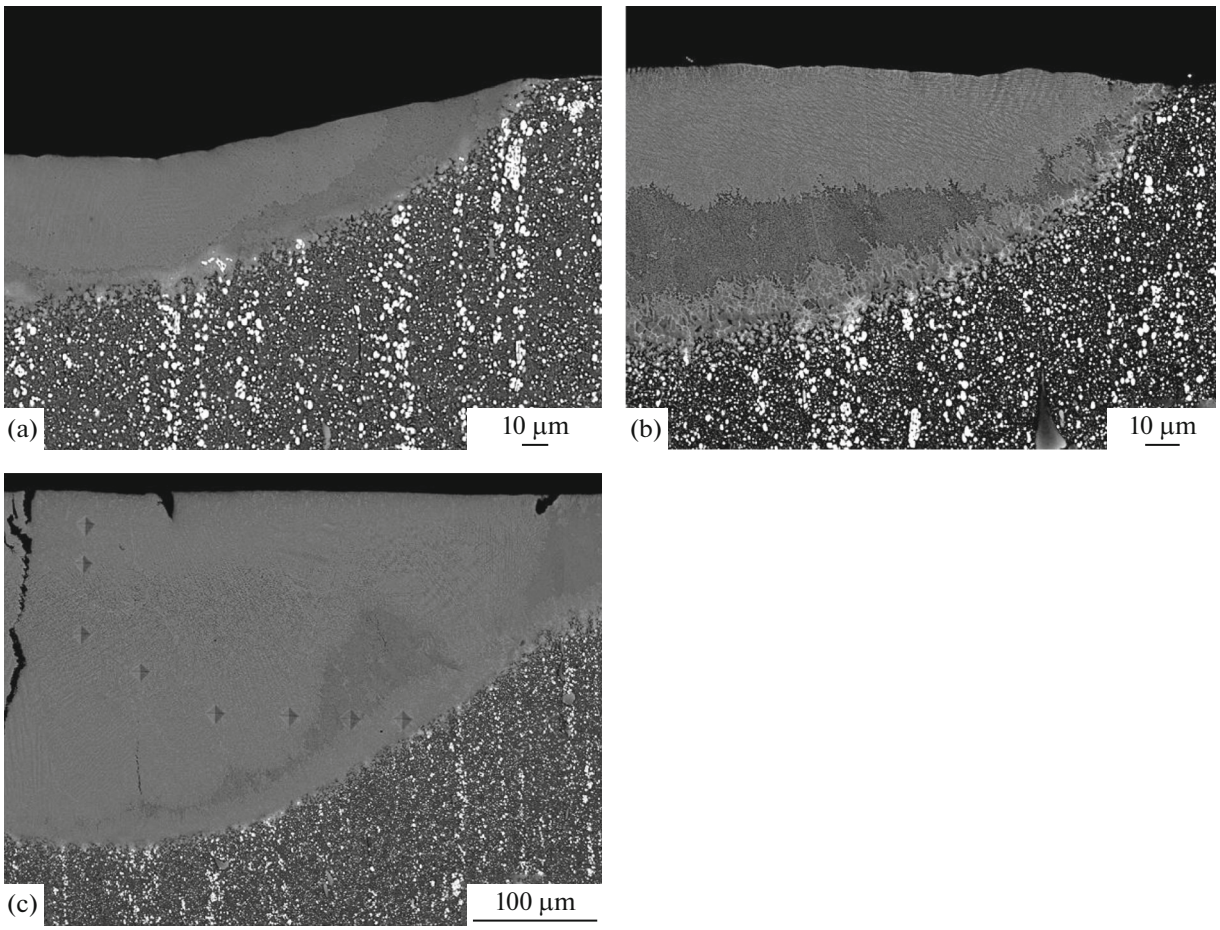

Fig. 3. Overall view of the LAZs in (a) O1, (b) O2, and (c) O3 samples.

bides precipitated along the cell boundaries is 20–30 nm (see Fig. 4b).

The regions of the well-etchable dendrites in these samples (Figs. 4e, 4f, respectively) have a higher degree of dispersion of both dendritic cells and of carbides in comparison with similar regions observed in all the samples of the heat-treated HSS after the same LT [33]. All this demonstrates the higher rate of crystallization in the RMZ of the annealed HSS. On the other hand, likely for this reason, a microporosity appears in the RMZ of samples of the O1 series, which was absent in the microstructure of the heat-treated HSS [33]. This microporosity is illustrated by the example of O1 and O3 samples (see Fig. 4). In addition, as shown in Fig. 3c, the central part of the RMZ of the O3 sample contains a large crack running perpendicularly from the surface through almost the entire zone, which may also be due to the higher rate of crystallization of the melt in the RMZ of this sample.

As in the case of the heat-treated HSS [33], the microstructure of the RMZ of samples of the series O after LT is mainly represented by high-alloy austenite and by a smaller amount of structureless martensite. According to the data of the metallographic analysis using a NIS-Elements software, the volume fraction of austenite in the steel matrix in the RMZ after LT was 96–98% for the O1 and O2 samples, and about 60% for the O3 sample. These features of the micro-

Table 2. Depth and width of the LAZ, microhardness of the basic metal and of the remelting zone in the samples studied

Sample	Depth, μm	Width, μm	Microhardness, HV	
			Basic metal	Remelting zone
O1	83	1497	272 ± 31	699 ± 65
O2	235	1452		696 ± 63
O3	280	1196		763 ± 75

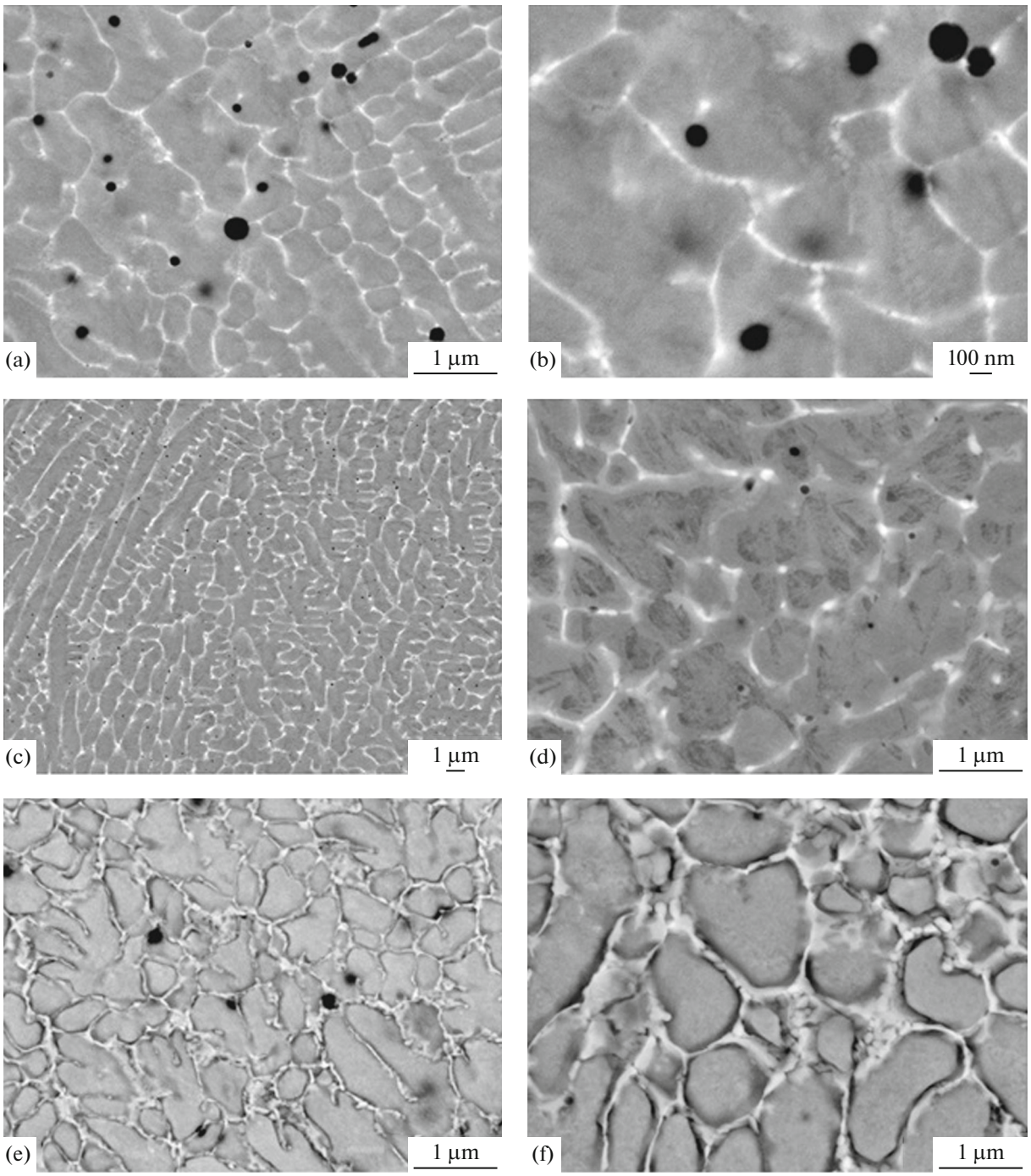

Fig. 4. Microstructure of the high-speed steel in the RMZ of (a, b, e) O1 and (c, d, f) O3 samples.

structure of experimental samples are also shown in Fig. 4.

The results obtained are in good agreement with the data of [35], according to which almost 100% of residual austenite was observed in the microstructure of the steel after LT with different values of the energy of laser irradiation (0.8 and 1.2 kW) and scanning velocity (25, 65, and 85 mm/s). It was shown in [36] that the volume fraction of austenite in the microstructure of the tool steel after LT also reached almost 100%. It is important that the authors of the last work believe that the formation of such a large amount of austenite is associated with the refinement of the dendritic structure of the steel matrix under the effect of the high cooling rate rather than with an increase in the carbon content and in the degree of alloying of the solid solution. It should be noted in this regard that

Table 3. Content of carbon and alloying elements in the matrix of samples in the RMZ after LT as compared to the matrix of the P6M5 steel subjected to standard heat treatment

Sample	Content of elements, wt %					
	C[1]	V	Cr	Fe	Mo	W
P6M5 without LT	2.09	1.19	3.48	85.72	3.23	4.29
O1	2.67	1.23	4.00	82.63	3.80	5.67
O2	3.10	1.22	4.08	81.60	4.03	5.97
O3	3.56	1.32	4.29	80.38	4.24	6.21

[1] Semiquantitative analysis.

using energy-dispersive X-ray spectroscopy, we found that the content of carbon and of the alloying elements in the steel matrix in the RMZ after LT is significantly higher than that in the matrix of the P6M5 steel subjected to standard heat treatment. With an increase in the energy of laser irradiation and in the duration of laser pulse, the content of carbon and alloying elements in the matrix increased slightly, as evidenced by the data given in Table 3. Thus, the smallest amount of residual austenite was found in sample O3, which is characterized by the highest degree of alloying of the solid solution. This result confirms the conclusions made in [36] on the secondary role of the degree of alloying of the solid solution during laser treatment from the viewpoint of the effect on the stabilization of austenite.

In all the samples of the O series, transition zones (TZ) are observed whose typical microstructure is shown in Fig. 5. The upper part of the TZ contains fine slightly elongated grains of the solid solution, which are surrounded by a developed network of eutectic carbides (Figs. 5a, 5b). A very high degree of

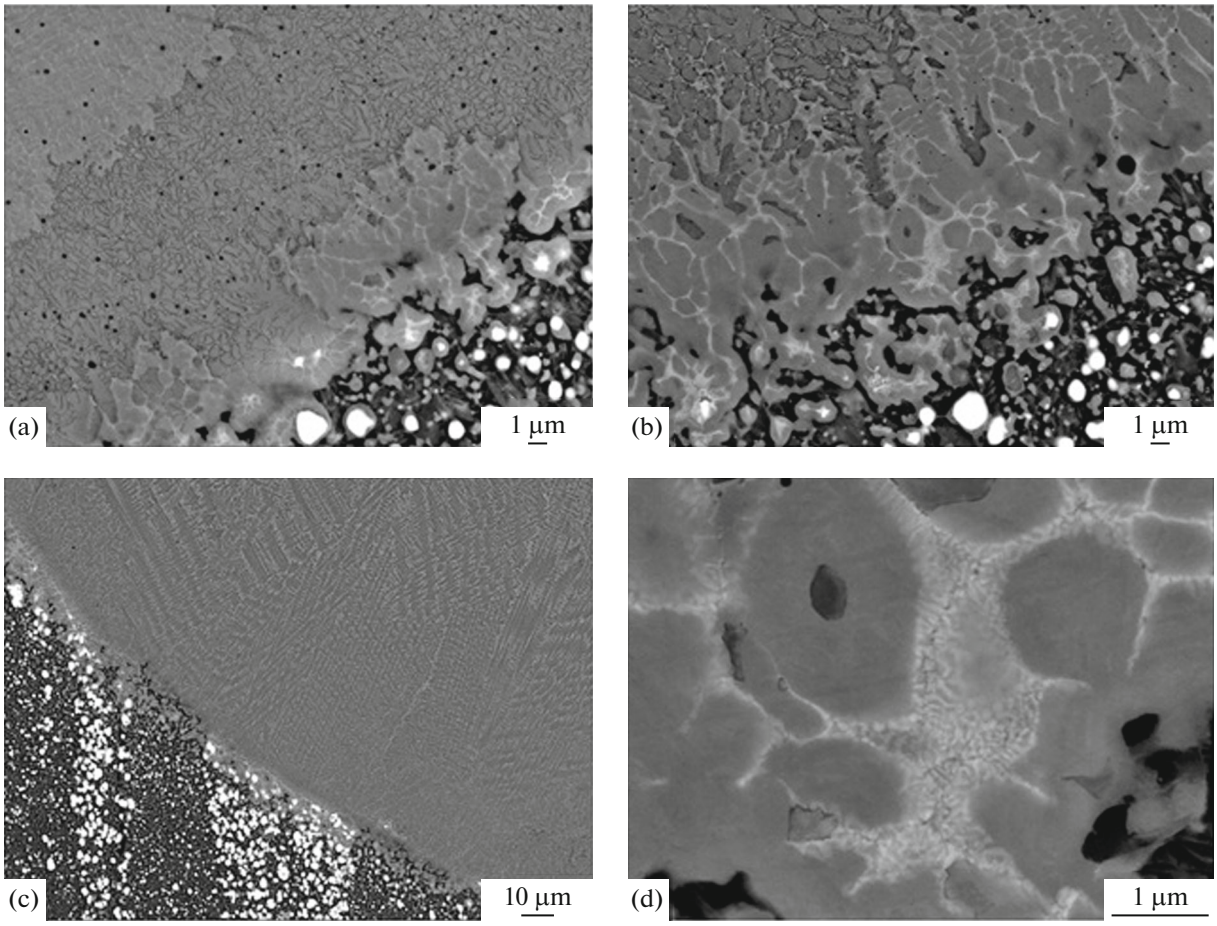

Fig. 5. Overall view of the microstructure of the boundary of the transition zone of the high-speed steel: basic metal in (a) O1, (b) O2, and (c) O3 samples, and (d) a fragment of the fine-structure eutectic that was formed in the transition zone of the sample O2.

dispersion of the eutectic constituent locally formed instead of the remelted particle of the initial eutectic carbide, presumably M_6C, is observed in Fig. 5d for sample O2. In the bottom part of the TZ, there are partially remelted grains of initial eutectic carbides, along the perimeter of which fine concentric layers of the high-alloy metal are observed (Figs. 5a, 5b).

In contrast to the heat-treated HSS [33], there are no heat-affected zones in the samples of the as-annealed steel (Figs. 5a–5c). The absence of the heat-affected zone in the annealed basic metal (BM) could be related to a significantly higher (by a factor of 1.5–2) thermal conductivity of the annealed HSS as compared to the quenched one. As a result, the heat releasing in the HAZ is quickly drawn-off into the BM and is dissipated there.

The microhardness values for the BM and for the upper part of the RMZ of samples of the series O are given in Table 2. The microhardness of the BM after LT is 272 ± 31 HV, while in the RMZ the microhardness is significantly higher in all the samples studied (see Table 2). However, the highest hardness was detected in the case of sample O3, which was significantly superior to samples O1 and O2. This is in good agreement with the data of metallographic analysis. The increased hardness of the sample O3 can be explained by the presence of a significantly smaller volume fraction of residual austenite in its microstructure.

It should be noted that the difference in the microhardness of the RMZ of the as-annealed samples, which depends on the laser-irradiation regimes and did not exceed 67 HV (Table 2), is smaller than that in samples of the heat-treated HSS (which was 287 HV) [33]. This indicates a lesser effect of LT regimes on the formation of the microstructure of the LAZ in the case of the annealed HSS as compared to heat-treated one, which may be associated with different thermal conductivity of the HSS in annealed and heat-treated states.

CONCLUSIONS

The effect of time and energy parameters of the pulsed LT on the structure formation and hardness of the P6M5-type HSS upon surface melting after annealing has been studied. The performed studies revealed the following regularities.

(1) The laser remelting leads to a significant refinement of grains of the matrix and of the carbide constituent of the annealed HSS. In this case, a higher degree of dispersion of the microstructure is achieved in the annealed steel as compared to as-heat-treated HSS. This may be associated with a higher rate of crystallization of the remelted metal, which is caused by the better thermal conductivity of the annealed steel.

(2) In the RMZ of the annealed HSS, the poorly etchable columnar dendrites with signs of directional crystallization dominate. The fraction of the compact arbitrarily oriented and well-etchable dendrites is much smaller in all the samples studied, which also indicates a higher rate of crystallization of the remelted metal in the case of annealed HSS as compared to the heat-treated analog. The microstructure of the RMZ of the samples studied is mainly formed by high-alloy austenite and structureless martensite.

(3) The upper part of the TZ contains regions of locally remelted initial particles of eutectic carbides with fine equiaxed solid-solution grains formed instead, which are surrounded by a developed network of dispersed eutectic carbides. The partially remelted grains of initial eutectic carbides, along the perimeter of which there are fine concentric layers of the high-alloy metal with a high degree of alloying, are located at the bottom part of the TZ.

(4) In contrast to the heat-treated HSS [33], the heat-affected zones in samples of the steel with the initial annealed state are absent, which may be due to the significantly higher (by 1.5–2 times) thermal conductivity of the annealed HSS as compared to quenched HSS.

(5) The LT of samples of the O series is accompanied by a significant increase in the microhardness of the metal in the RMZ (from 684 to 762 HV) as compared to the BM (272 HV*)* in the annealed state. The difference in the microhardness of the RMZ depending on the regimes of laser irradiation did not exceed 67 HV.

FUNDING

The work was supported by the VEGA projects (no. 1/0520/15 and APVV-16-0057), APRODIMET project (ITMS:26220120048), and the Research & Development Operational Program funded by the ERDF. J. Vidlička participated in this work.

REFERENCES

1. K. Bobzin, "High-performance coatings for cutting tools," CIRP J. Manuf. Sci. Technol. **18**, 1–9 (2017).
2. F. D. Gelin and A. S. Chaus, *Metallic Materials* (Vysheishaya shkola, Minsk, 2007) [in Russian].
3. V. P. Astakhov, "Tribology of cutting tools," in *Tribology in Manufacturing Technology*, Ed. by P. J. Davim (Springer, New York, 2013), pp. 1–66.
4. S.-H. Chang, T.-C. Tang, K.-T. Huang, and C.-M. Liu, "Investigation of the characteristics of DLC films on oxynitriding-treated ASP23 high speed steel by DC-pulsed PECVD process," Surf. Coat. Technol. **261**, 331–336 (2015).
5. M. Gowri, W. J. P. Enckevort, J. J. Schermer, J. P. Celis, J. J. Meulen, and J. G. Buijnsters, "Growth and adhesion of hot filament chemical vapor deposited diamond coatings on surface modified high speed steel," Diam. Relat. Mater. **18**, 1450–1458 (2009).
6. R. Polini, Mantini F. Pighetti, M. Braic, M. Amar, W. Ahmed, and H. Taylor, "Effects of Ti- and Zr-based

interlayer coatings on the hot filament chemical vapour deposition of diamond on high speed steel," Thin Solid Films **494**, 116–122 (2006).

7. L. Schäfer, M. Fryda, T. Stolley, L. Xiang, and C.-P. Klages, "Chemical vapour deposition of polycrystalline diamond films on high-speed steel," Surf. Coat. Technol. **116–119**, 447–451 (1999).
8. W. Wu, W. Chen, S. Yang, Y. Lin, S. Zhang, T-Y. Cho, G. H. Lee, and S-Ch. Kwon, "Design of AlCrSiN multilayers and nanocomposite coating for HSS cutting tools," Appl. Surf. Sci. **351**, 803–810 (2015).
9. I. S. Cho, A. Amanov, and J. D. Kim, "The effects of AlCrN coating, surface modification and their combination on the tribological properties of high speed steel under dry conditions," Tribol. Int. **81**, 61–72 (2015).
10. D. Kottfer, M. Ferdinandy, L. Kaczmarek, I. Maňková, and J. Beňo, "Investigation of Ti and Cr based PVD coatings deposited onto HSS Co 5 twist drills," Appl. Surf. Sci. **282**, 770–776 (2013).
11. J. Gerth and U. Wiklund, "The influence of metallic interlayers on the adhesion of PVD TiN coatings on high-speed steel," Wear **264**, 885–892 (2008).
12. A. S. Chaus, P. Pokorný, L' Čaplovič, M. V. Sitkevich, and J. Peterka, "Complex fine-scale diffusion coating formed at low temperature on high-speed steel substrate," Appl. Surf. Sci. **437**, 257–270 (2018).
13. M. G. Krukovich, B. A. Prusakov, and I. G. Sizov, *Plasticity of Boronized Layers*, in Springer Series in Materials Science, Vol. 237 (Springer, 2016).
14. B. Edenhofer, D. Joritz, M. Rink, and K. Voges, "Carburizing of steels," in *Thermochemical Surface Engineering of Steels*, Ed. by E. J. Mittemeijer and M. A. J. Somers (Woodhead Publishing, 2015).
15. E. D. Doyle, A. M. Pagon, P. Hubbard, S. J. Dowey, A. Pilkington, and D. G. McCulloch, "Nitriding of high speed steel," Int. Heat Treat. Surf. Eng. **5**, 69–72 (2011).
16. A. S. Chaus, M. Murgas, I. V. Latyshev, and R. Toth, "Heat treatment of cast carburising high-speed steel alloyed with Ti, Nb and V," Met. Sci. Heat Treat. **43**, 220–223 (2001).
17. Yu. A. Geller, *Instrumental Steels* (5th Ed.) (Metallurgiya, Moscow, 1983) [in Russian].
18. N. Hashemi, A. Mertens, H.-M. Montrieux, J. T. Tchuindjang, O. Dedry, R. Carrus, and J. Lecomte-Beckers, "Oxidative wear behaviour of laser clad high speed steel thick deposits: Influence of sliding speed, carbide type and morphology," Surf. Coat. Technol. **315**, 519–529 (2017).
19. G. F. Sun, K. Wang, R. Zhou, A. X. Feng, and W. Zhang, "Effect of different heat-treatment temperatures on the laser clad M3:2 high-speed steel," Mater. Des. **65**, 606–616 (2015).
20. P. A. Ogin, D. L. Merson, L. A. Kondrashina, and K. Ya. Vas'kin, "The influence of laser modification modes on the structure, properties, and wear resistance of small-sized high-speed R6M5 steel tools," Vektor Nauki TGU, No. 4, 83–88 (2015).
21. L. E. Afanas'eva, I. A. Barabonova, E. V. Botyanov, G. V. Ratkevich, and R. M. Grechishkin, "Structural phase transitions in high-speed steel upon laser quenching with surface melting treatment using a multichannel CO_2 laser," Uprochn. Tekhnol. Pokryt. No. 8, 10–13 (2013).
22. P. Jurči, J. Cejp, and J. Brajer, "Metallurgical aspects of laser surface processing of PM Cr–V ledeburitic steel," Adv. Mater. Sci. Eng. **2011**, 1–8 (2011).
23. J. Arias, M. Cabeza, G. Castro, I. Feijoo, P. Merino, and G. Pena, "Microstructural characterization of laser surface melted AISI M2 tool steel," J. Microsc. **239**, 184–193 (2010).
24. K. Y. Benyounis, O. M. Fakron, and J. H. Abboud, "Rapid solidification of M_2 high-speed steel by laser melting," Mater. Des. **30**, 674–678 (2009).
25. W. Darmawan, J. Quesada, and R. Marchal, "Characteristics of laser melted AISI-T1 high speed steel and its wear resistance," Surf. Eng. **23**, 112–119 (2007).
26. R. Colaço, E. Gordo, E. M. Ruiz-Navas, M. Otasevic, and R. Vilar, "A comparative study of the wear behaviour of sintered and laser surface melted AISI M42 high speed steel diluted with iron," Wear **260**, 949–956 (2006).
27. S. Kąc and J. Kusiński, "SEM and TEM microstructural investigation of high-speed tool steel after laser melting," Mater. Chem. Phys. **81**, 510–512 (2003).
28. G. H. Shehata, A. M. A. Moussa, and P. Molian, "A Nd:YAG laser alloying of high-speed steel tools with BN and Ti/BN and the effects on turning performance," Wear **179**, 199–210 (1993).
29. A. G. Grigor'yants, *Fundamentals of Laser Treatment of Materials* (Mashinostroenie, Moscow, 1989) [in Russian].
30. C. Soriano, J. Leunda, J. Lambarri, Navas V. Garcia, and C. Sanz, "Effect of laser surface hardening on the microstructure, hardness and residual stresses of austempered ductile iron grades," Appl. Surf. Sci. **257**, 7101–7106 (2011).
31. J. Sander, J. Hufenbach, L. Giebeler, H. Wendrock, U. Kühn, and J. Eckert, "Microstructure and properties of FeCrMoVC tool steel produced by selective laser melting," Mater. Des. **89**, 335–341 (2016).
32. Z. H. Liu, D. Q. Zhang, C. K. Chua, and K. F. Leong, "Crystal structure analysis of M2 high speed steel parts produced by selective laser melting," Mater. Charact. **84**, 72–80 (2013).
33. A. S. Chaus, A. V. Maksimenko, N. N. Fedosenko, Ľ. Čaplovič, and V. N. Myshkovets, "Formation of structure of a high-speed steel upon laser surface melting," Phys. Met. Metallogr. **120**, 269–277 (2019).
34. A. S. Chaus, "Structural and phase changes in carbides of the high-speed steel upon heat treatment," Phys. Met. Metallogr. **117**, 684–692 (2016).
35. C. T. Kwok, K. H. Lo, F. T. Cheng, and H. C. Man, "Effect of processing conditions on the corrosion performance of laser surface-melted AISI 440C martensitic stainless steel," Surf. Coat. Technol. **166**, 221–230 (2003).
36. R. Colaço and R. Vilar, "Stabilisation of retained austenite in laser surface melted tool steels," Mater. Sci. Eng., A **385**, 123–127 (2004).

Translated by O. Golosova